Invariance and proportional scaling in axonal conduction

Laurie D. Cohen and Shimon Marom
Technion—Israel Institute of Technology, Haifa 32000, Israel
(Dated: October 23, 2025)

Conduction velocity along axons depends on geometric and biophysical factors whose *collective* statistical organization has remained unexplored. Using high-resolution time-of-arrival measurements along hundreds of identified cortical axonal branches, we quantified how propagation speed changes along trajectories. The ratio between terminal and initial velocities, $\rho = v_{\mathrm{end}}/v_{\mathrm{start}}$, follows a right-skewed distribution that remains stable across branch lengths, geometries, and positions within neurons. The pattern accords with stochastic transport in disordered media, where local variations compound multiplicatively to yield characteristic right-skewed statistics. Spatial embedding thus preserves the proportional organization of excitability, ensuring reliable transmission in a structurally variable substrate.

Several studies of the biophysical mechanisms underlying membrane excitability have converged toward a view of the excitable membrane as a self-organizing system whose kinetics exhibit scaling relations and functional resilience across wide ranges of structural variability [1–13]. These analyses, based on single-protein and whole-cell observations, suggest that reliable excitability arises from the collective kinetics of interacting conductances rather than from fixed molecular architecture. Here we ask whether such scale-invariant properties extend to spatially distributed settings; conduction velocity along axons providing a simple test case.

Conduction velocity is a fundamental property of excitable media. In neuronal axons, it depends on geometry, membrane protein density, and multiple state-dependent processes that generate local variations in propagation speed [13–23]. Such variations can yield distinct macroscopic outcomes: if structural and kinetic factors balance geometric and branching effects, velocity remains invariant; if they do not, conduction may accelerate or slow along the trajectory. It may also vary idiosyncratically, reflecting unpredictable local contingencies.

We report that axonal conduction slows down systematically along axonal trajectories. The slowdown is not idiosyncratic but follows a statistical regularity. Specifically, the ratio of end-to-start velocities is distributed lognormally across hundreds of axonal segments. This observation indicates that conduction slowdown is shaped by multiplicative influences, extending current analyses of specific determinants toward a broader identification of the stochastic processes that govern axonal propagation. Such proportional scaling laws are familiar in transport through disordered or heterogeneous media, where local fluctuations compound multiplicatively to yield lognormal behavior [24–27].

All experiments were performed in *ex vivo* developing cortical networks, as described elsewhere [9, 28, 29]. Recordings were obtained with CMOS-based high-density multielectrode arrays (HD-MEAs; *MaxWell Biosystems* AG), a non-invasive platform enabling reconstruction of axonal trajectories from electrical activity [17, 30–32]. Axonal branches were identified with the *AxonTracking* module of the *MaxLab Live* software, which links sequential electrodes exhibiting time-shifted spike-triggered averages consistent with continuous extracellular conduction along axonal processes (Figure 1). For each identified axonal branch, time of arrival (TOA) to a given point along the branch was defined as the latency of spike detection at the corresponding electrode relative to the soma. TOA–distance relationships were fitted by ordinary least squares over the first and last 20% of sam-

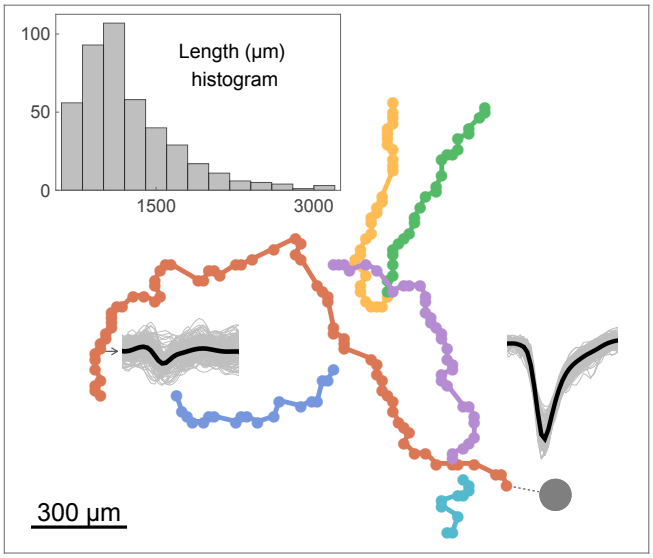

FIG. 1. Axonal trajectories were identified using the *AxonTracking* module of *MaxLab Live*. The gray circle marks the site of somatic spike initiation, and the dashed line indicates the direction of propagation. Colored dots mark electrode positions underlying reconstructed paths. Representative voltage traces (thin lines, single events; thick lines, averages; trace duration $\sim$ 1.5 ms) illustrate a somatic spike followed by a spike in one distal axonal electrode $\sim$ 3.9 ms later. Scales: mean somatic spike amplitude, $\sim$ 600 μV; typical mean axonal spike amplitude, 4–15 μV. The inset shows the distribution of branch lengths in the dataset (431 branches from 248 neurons across 14 networks).

pled points (minimum five points per segment). Branches were retained only if both fits achieved $R^2 \geq 0.95$ and the ratio of end-to-start velocities, $\rho = v_{\text{end}}/v_{\text{start}}$, satisfied $0 < \rho < 2.5$. After screening, the dataset comprises 431 branches of length (L) ranging from 600 μm to 4570 μm, recorded from 248 different neurons across 14 networks. All statistical analyses were performed in Mathematica and Python using custom scripts.

Before analyzing the statistical form of ρ, we asked whether its variability might reflect differences in axonal length or the number of branching points along the way (which, in our data, are highly correlated; $r > 0.88$ [29]). Across all 431 branches, there was no relationship between branch length and ρ (Pearson $r = 0.018$, $p = 0.71$; Spearman coefficient $= 0.044$, $p = 0.36$). This result rules out geometric sampling bias as a source of the observed ρ variability and indicates that any systematic structure in the distribution of ρ must arise from intrinsic dynamical factors rather than measurement or morphological confounds.

Four examples of TOA–distance relationships are shown in Figure 2, along with linearly fitted functions for estimation of end-to-start velocities, $\rho = v_{\text{end}}/v_{\text{start}}$. Log-log insets emphasize the continuous nature of TOA–distance relationship. In all four exemplar cases of Figure 2, a slowdown phenomenon ($\rho < 1$) is clearly visible.

The distribution of ρ across 431 branches (Figure 3) is skewed, with typical branches slow by $\sim 30\%$ (mean $\rho \approx 0.70$, median $\rho \approx 0.68$), and a right tail for rare acceleration (approximately 6% of branches exhibiting $\rho > 1$).

As an additional diagnostic, we examined the ratio between the average and initial conduction velocities for

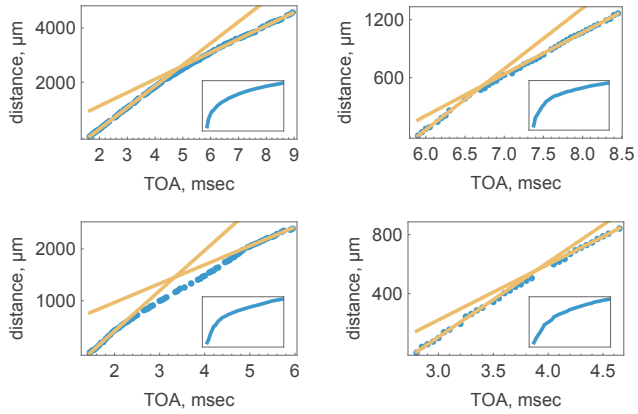

FIG. 2. Time-of-arrival (TOA) versus distance for representative axonal branches, with linear fits to the initial and terminal segments used to estimate start and end conduction velocities, v_{start} and v_{end}. Insets show the same data on log-log axes, emphasizing the smooth, continuous nature of the TOA–distance relationships. The two bottom panels correspond to segments from the neuron of Figure 1.

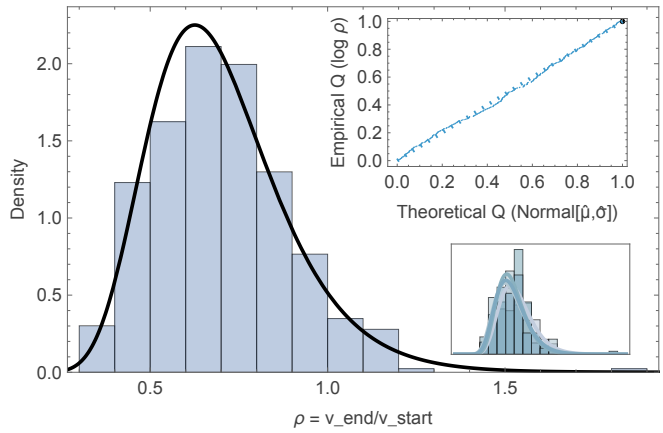

FIG. 3. Distribution of conduction velocity ratios, $\rho = v_{\text{end}}/v_{\text{start}}$, across 431 axonal branches. The solid line shows the maximum-likelihood log-normal fit ($\hat{\mu} = -0.3943$, $\hat{\sigma} = 0.2729$; median $\rho \approx 0.68$), representative of proportional compounding models. *Top Inset*: Quantile–quantile (Q–Q) plot comparing ordered empirical $\log \rho$ values with expected quantiles of $N(\hat{\mu}, \hat{\sigma})$; the near-linear alignment indicates that $\log \rho$ closely follows a normal distribution, i.e. ρ is log-normally distributed. *Bottom inset*: Stratification by branch initial spike time (a proxy for distance from soma) shows stable distributional shape ($\hat{\sigma} \approx 0.25$–$0.28$) and a modest distal shift in central tendency (median ρ increasing from ~ 0.64 to ~ 0.75).

each branch, denoted $\bar{\rho}_s = v_{\text{average}}/v_{\text{start}}$, and the ratio between the end and average conduction velocities, denoted $\bar{\rho}_e = v_{\text{end}}/v_{\text{average}}$. These measures provide a complementary view to the end-to-start ratio ($\rho = v_{\text{end}}/v_{\text{start}}$), summarizing the overall slowing along the trajectory. Across all branches, $\bar{\rho}$ exceeded ρ ($\langle \bar{\rho}_s \rangle \approx 0.88$ and $\langle \bar{\rho}_e \rangle \approx 0.79$ vs. $\langle \rho \rangle \approx 0.69$), suggesting that the slowdown is progressive and monotonic rather than step-like. The distributions of $\bar{\rho}_s$ and $\bar{\rho}_e$ were likewise right-skewed, with approximately 18% and 10% of branches, respectively, exhibiting values greater than unity. These findings confirm that the overall deceleration is gradual and systematic, and that the statistical regularity captured by ρ reflects a monotonic compounding process rather than discrete local fluctuations.

A maximum-likelihood estimation yields $\log \rho \sim \mathcal{N}(\hat{\mu}, \hat{\sigma})$, $\hat{\mu} = -0.3943$, $\hat{\sigma} = 0.2729$, implying median $\hat{\rho} = e^{\hat{\mu}} \approx 0.674$ and mean $\hat{\rho} \approx 0.70$, closely matching empirical values. 95% bootstrap confidence intervals (CI_{95}) were estimated for the log-normal parameters (μ, σ) and the median of ρ using 2000 resamples, yielding $\mu \in [-0.42, -0.37]$, $\sigma \in [0.26, 0.29]$, and median $\rho \in [0.66, 0.69]$. The Q–Q plots for $\log \rho$ (top inset to Figure 3) are near-linear with minor deviations.

To verify that the observed log-normal form of slowdown is not an artifact of model choice, we performed a series of robustness checks. To encompass the main mechanistic possibilities, we examined three representative families—the *Gamma*, *log-normal*, and *log-logistic*

distributions, providing a minimal yet comprehensive basis for assessing which process best accounts for the observed form of ρ. Information criteria favored the log-normal model (AIC $= -232.18$; BIC $= -224.05$), with the Gamma distribution close behind (ΔAIC $= \Delta$BIC $=$ 1.31) and therefore statistically indistinguishable. However, the Gamma family represents an additive generative process, in which variability accumulates through independent increments. This is not physiologically well grounded: excitability mechanisms, particularly sodium conductance, gating kinetics, and local impedance interactions, operate through proportional effects on current and voltage, not through additive time delays. The log-logistic model performed poorly (ΔAIC $= \Delta$BIC $=$ 12.86), providing no credible support for a regulated-multiplicative process. For completeness, we also fitted an *extreme-value* (Gumbel) distribution, which yielded ΔAIC $= \Delta$BIC $= 6.36$ relative to the log-normal. Although this difference is marginally acceptable statistically, an extreme-value process is mechanistically more difficult to reconcile with the data: The smooth convexity of time-of-arrival relations, the independence of ρ from branch length, and the near-normal distribution of $\log \rho$ all indicate that slowdown arises from the compounded effect of many small influences rather than from a bottleneck along the axon.

To examine whether hierarchical dependencies among branches, neurons, and networks influence the observed distribution of conduction slowdown, we aggregated ρ values at successive levels and re-fitted the log-normal model to each aggregate. At the neuron level, branch-specific ρ values were averaged to yield one representative value per neuron, and at the network level, neuron means were further averaged to produce one value per network. The fitted parameters remained stable across levels: Branch level (reported above): $\mu = -0.39$, $\sigma = 0.27$; Neuron level: $\mu = -0.40$, $\sigma = 0.24$; Network level: $\mu = -0.40$, $\sigma = 0.13$). The corresponding medians (≈ 0.67) and means (≈ 0.69) were nearly invariant. The constancy of μ and the median indicates that the central tendency of slowdown is invariant to aggregation. The mild reduction of σ with aggregation reflects within-neuron and within-network correlations of modest magnitude. Thus, clustering exists but does not distort the log-normal form nor the overall 30% slowdown ratio.

Finally, stratification by branch initial spike time (Figure 3, bottom inset), a proxy for branch position relative to the soma, showed stable distributional shape ($\hat{\sigma} \approx 0.25$–$0.28$) and a modest distal shift in central tendency (median ρ increasing from ~ 0.64 to ~ 0.75).

Together, the above analyses demonstrate that the slowdown pattern represents a statistical regularity rather than a consequence of a particular fitting scheme. The single log-normal form is parsimonious and robust across analytic choices and spatial scales.

Having established these empirical regularities, we turn to their mechanistic and physiological implications. The observed invariance of conduction slowdown to geometric scale and structural detail indicates that propagation speed is governed by a scale-preserving stochastic process in which local influences compound to produce a right-skewed distribution that remains stable across branches, neurons, and networks. The essential empirical constraint is the invariance itself: any viable mechanistic account must reproduce the stability of the distribution under structural diversity. This behavior is consistent with, though not exclusive to, multiplicative dynamics, in which each axonal segment rescales velocity by a fractional factor reflecting its geometry or biophysical state, with the cumulative effect yielding the observed statistical form.

Processes of this sort are familiar from stochastic transport in disordered media, where numerous small influences combine to generate log-normal or related right-skewed distributions. In axons, several mechanisms could instantiate such invariance: current splitting at bifurcations, impedance mismatches, gradual diameter taper, or slow, state-dependent channel kinetics. None of these mechanisms are mutually exclusive; together they may define the effective stochastic law governing propagation.

A particularly relevant example is the slow inactivation of voltage-gated sodium channels, whose fractional availability is activity-dependent over wide temporal scales [4, 33]. Because channel gating enters multiplicatively into total sodium conductance, variations in availability modulate conductance proportionally. Since conduction velocity scales with instantaneous sodium conductance, such proportional modulation can compensate for structural variability and support robust function.

From a physiological standpoint, the robustness of conduction to structural variability is fundamental. Neural tissue operates within a geometrically irregular and dynamically mutable medium, where precise architectural reproducibility is neither attainable nor required. That axonal propagation remains statistically invariant despite such variability implies that the organization of excitability is tuned for functional reliability rather than for precision of structure. Proportional or self-normalizing regulation ensures that local differences in geometry or conductance compound without degrading transmission fidelity. Conduction dynamics are stabilized by the same scale-preserving organization that sustains excitability itself, enabling faithful signal transmission in a structurally heterogeneous substrate.

The authors thank Tamar Galateanu and Leonid Odessky for technical assistance, and Erez Braun, Naama Brenner, and Hana Salman for insightful discussions. This work was partially supported by the Schaefer Scholars Program at Columbia University's Vagelos College of Physicians and Surgeons.

[1] G. Millhauser, E. Salpeter, and R. Oswald, Diffusion models of ion-channel gating and the origin of power-law distributions from single-channel recording, Proceedings of the National Academy of Sciences **85**, 1503 (1988).

[2] M. Teich, Fractal character of the auditory neural spike train, IEEE Transactions on Biomedical Engineering **36**, 150 (1989).

[3] L. Liebovitch and T. Tóth, Distributions of activation energy barriers that produce stretched exponential probability distributions for the time spent in each state of the two state reaction, Bulletin of Mathematical Biology **53**, 443 (1991).

[4] A. Toib, V. Lyakhov, and S. Marom, Interaction between duration of activity and time course of recovery from slow inactivation in mammalian brain Na^+ channels., J. Neurosci. **18**, 1893 (1998).

[5] S. Lowen, L. Liebovitch, and J. White, Fractal ion-channel behavior generates fractal firing patterns in neuronal models, Physical Review E **59**, 5970 (1999).

[6] R. K. Ellerkmann, V. Riazanski, C. E. Elger, B. W. Urban, and H. Beck, Slow recovery from inactivation regulates the availability of voltage-dependent sodium channels in hippocampal granule cells, hilar neurons and basket cells, J Physiol **532**, 385 (2001).

[7] E. Marder, Variability, compensation, and modulation in neurons and circuits, Proceedings of the National Academy of Sciences **108**, 15542 (2011).

[8] I. Goychuk and P. Hanggi, Fractional diffusion modeling of ion channel gating, Physical Review E **70**, 051915 (2004).

[9] A. Gal, D. Eytan, A. Wallach, M. Sandler, J. Schiller, and S. Marom, Dynamics of excitability over extended timescales in cultured cortical neurons, J. Neurosci. **30**, 16332 (2010).

[10] A. Gal and S. Marom, Self-organized criticality in single-neuron excitability, Physical Review E **88**, 062717 (2013).

[11] C. Meisel, A. Klaus, C. Kuehn, and D. Plenz, Critical slowing down governs the transition to neuron spiking, PLoS computational biology **11**, e1004097 (2015).

[12] S. Marom, Emergence and maintenance of excitability: kinetics over structure, Current Opinion in Neurobiology **40**, 66 (2016).

[13] S. Marom and E. Marder, A biophysical perspective on the resilience of neuronal excitability across timescales, Nature Reviews Neuroscience **24**, 640 (2023).

[14] I. Segev and E. Schneidman, Axons as computing devices: Basic insights gained from models, Journal of Physiology-Paris **93**, 263 (1999).

[15] D. Bucher and J.-M. Goaillard, Beyond faithful conduction: short-term dynamics, neuromodulation, and long-term regulation of spike propagation in the axon, Progress in Neurobiology **94**, 307 (2011).

[16] D. Debanne, E. Campanac, A. Bialowas, E. Carlier, and G. Alcaraz, Axon physiology, Physiological Reviews **91**, 555 (2011).

[17] D. J. Bakkum, U. Frey, M. Radivojevic, T. L. Russell, J. Müller, M. Fiscella, H. Takahashi, and A. Hierlemann, Tracking axonal action potential propagation on a high-density microelectrode array across hundreds of sites, Nature Communications **4**, 2181 (2013).

[18] A. El Hady and B. B. Machta, Mechanical surface waves accompany action potential propagation, Nature Communications **6**, 6697 (2015).

[19] S. Rama, M. Zbili, and D. Debanne, Signal propagation along the axon, Current Opinion in Neurobiology **51**, 37 (2018).

[20] P. Alcami and A. El Hady, Axonal computations, Frontiers in Cellular Neuroscience **13** (2019).

[21] V. Emmenegger, M. E. J. Obien, F. Franke, and A. Hierlemann, Technologies to study action potential propagation with a focus on HD-MEAs, Frontiers in Cellular Neuroscience **13** (2019).

[22] H. Kamiya and D. Debanne, Axon neurobiology: fine-scale dynamics of microstructure and function, Frontiers in Cellular Neuroscience **14** (2020).

[23] Y. Zang, E. Marder, and S. Marom, Sodium channel slow inactivation normalizes firing in axons with uneven conductance distributions, Current Biology **33**, 1818 (2023).

[24] R. Landauer, Electrical resistance of disordered one-dimensional lattices, Philosophical Magazine **21**, 863 (1970).

[25] S. Kirkpatrick, Percolation and conduction, Reviews of Modern Physics **45**, 574 (1973).

[26] J.-P. Bouchaud and A. Georges, Anomalous diffusion in disordered media: statistical mechanisms, models and physical applications, Physics Reports **195**, 127 (1990).

[27] E. Limpert, W. A. Stahel, and M. Abbt, Log-normal distributions across the sciences: keys and clues, BioScience **51**, 341 (2001).

[28] D. Eytan and S. Marom, Dynamics and effective topology underlying synchronization in networks of cortical neurons, J. Neurosci. **26**, 8465 (2006).

[29] L. D. Cohen, T. Galateanu, and S. Marom, Dynamics of excitability in axonal trees, bioRxiv (2025).

[30] J. Müller, M. Ballini, P. Livi, Y. Chen, M. Radivojevic, A. Shadmani, V. Viswam, I. L. Jones, M. Fiscella, R. Diggelmann, *et al.*, High-resolution CMOS MEA platform to study neurons at subcellular, cellular, and network levels, Lab on a Chip **15**, 2767 (2015).

[31] M. Radivojevic, F. Franke, M. Altermatt, J. Müller, A. Hierlemann, and D. J. Bakkum, Tracking individual action potentials throughout mammalian axonal arbors, Elife **6**, e30198 (2017).

[32] M. Radivojevic and A. Rostedt Punga, Functional imaging of conduction dynamics in cortical and spinal axons, eLife **12**, e86512 (2023).

[33] W. Ulbricht, Sodium channel inactivation: molecular determinants and modulation, Physiol. Rev. **85**, 1271 (2005).